Journal of ELECTRONIC MATERIALS, Vol. 49, No. 9, 2020
https://doi.org/10.1007/s11664-020-08280-x
© 2020 The Minerals, Metals & Materials Society

Synthesis of ZnO Ultra-Thin Film-Based Bottom-Gate Phototransistors for UV Detection

BASAVARAJ S. SANNAKASHAPPANAVAR,[1,2]
ANIRUDDH BAHADUR YADAV,[3,6,7] C.R. BYRAREDDY,[4]
and N.V.L. NARASIMHA MURTY[5]

1.—Visvesvaraya Technological University, Belagavi, Karnataka 590018, India. 2.—Department of Electronics and Telecommunication Engineering, Annasaheb Dange College of Engineering & Technology, Ashta, Maharashtra 416301, India. 3.—Department of Electronics and Communication Engineering, Velagapudi Ramakrishna Siddhartha Engineering College Kanuru, Vijayawada, Andhra Pradesh 520007, India. 4.—Department of Electronics and Communication Engineering, Bangalore Institute of Technology, Bangalore, Karnataka 560004, India. 5.—Department of Electrical Engineering, Indian Institute of Technology, Tirupati 517506, India. 6.—e-mail: ani84ani@gmail.com. 7.—e-mail: abyadav.rs.ece@itbhu.ac.in

The present study illustrates the fabrication of ZnO ultra-thin film (25 nm)-based bottom gate phototransistors using RF sputtering and thermal evaporation on SiO_2/Si substrate for UV detection. According to the literature, phototransistors have the ability to solve persistent photoconductivity (PPC). PPC increases the response time of metal oxide semiconductor-based conventional two-terminal photodetectors. Prior to transistor fabrication, the surface of the deposited ZnO thin film was treated with hydrogen peroxide (H_2O_2) in order to improve its crystal structure, surface morphology, energy bandgap, and electrical conductivity. The characteristics of ZnO thin film were investigated by atomic force microscope (AFM), field emission scanning electron microscopy (FESEM), x-ray diffraction (XRD), photoluminescence (PL), and x-ray photoelectron spectroscopy (XPS). The electrical and optical performance of phototransistors were investigated by measuring their output and transfer characteristics in dark and UV light. H_2O_2 treatment was found to be effective in producing efficient optical detection phototransistor. Optoelectronics properties (for UV detection) of the fabricated phototransistors were studied by using low-intensity and low power commercial LEDs of 365 nm wavelength.

Key words: ZnO thin film, bottom-gate phototransistor, RF sputtering, UV detection

INTRODUCTION

Recently, ultraviolet (UV) photosensors with low thickness (∼ 80 nm to 900 nm) ZnO thin film as their active channel have attracted the attention of many researchers. This is because of the unique properties of the ZnO thin film and the significant applications of UV photodetectors in the fields of UV sterilization, communication, radar, and imaging.[1–7] ZnO is a non-toxic, intrinsically *n*-type, low-cost and robust, metal-oxide semiconductor with wide energy bandgap (∼ 3.34 eV) and large exciton binding energy (∼ 60 meV) (providing lasing at room temperature). Thin films of ZnO have been synthesized by several low-cost deposition techniques for the fabrication of efficient UV photodetectors.[1–15] Many UV photodetectors using ZnO thin film as an active channel have already been reported in the literature. For instance, Shaikh

(Received September 7, 2019; accepted June 15, 2020; published online July 6, 2020)

et al.[1] have fabricated a metal–semiconductor–metal (MSM) structure for the detection of UV wavelength. This photodetector was fabricated using a nanoflower structured ZnO thin film (700–900 nm) as an active channel deposited by using a chemical bath. They observed that the film thickness had a great influence on the photo-sensing properties of their photodetector. Yadav et al.[5] synthesized a ZnO thin film (200 nm) by sol–gel spin coating for the fabrication of a Schottky diode-based photodetector. Hanna et al.[6] reported an Ag/NPB/ZnO/TiO_2/ITO/glass structure photodetector, wherein the active channel of this device was low-temperature processed ZnO thin film ($\sim$ 200 nm). Rajan et al.[7] deposited Pt interdigitated electrodes on sol–gel derived, silver doped ZnO thin film (221 nm thick) to fabricate the UV photodetector. Yadav et al.[11] reported an increase in the photosensitivity of an MSM-based photodetector by decreasing the thickness of the ZnO thin film which acts as an active channel. However, persistent photoconductivity (PPC) has severely degraded the recovery time of all these conventional two-terminal photodetectors. PPC is associated with the oxygen vacancies in ZnO, which induces conductivity in the semiconductor for several hours after the removal of light.[1,5–7] In view of this, phototransistors (PTs), three-terminal electronic devices, have recently been employed to eliminate the PPC from ZnO (used as an active channel) by applying negative pulses at their third terminal called a gate.[8] As a result, after the removal of the PPC, the response time of phototransistors was much improved.[8] Therefore, the use of phototransistors is found to be beneficial over the two-terminal devices. Lee et al.[8] reported enhancement in the photoresponse of a phototransistor, which has 80 nm thick ZnO thin film as an active channel with transparent source and drain electrodes. Liu and Huang[9] fabricated a fully transparent phototransistor with its photosensitivity better than fully or partially transparent phototransistors. In this case, the active channel of the phototransistor was an 80 nm mist atmospheric pressure chemical vapor deposition ZnO thin film. In another study, Lee et al.[10] improvement in the photodynamic properties of a phototransistor using 200 nm ZnO thin film as an active channel was observed. This improvement was attributed to the polymer dielectric gate. In all the above studies, the active channel thickness of photosensors (PT or two-terminal photodetector) was in the range of 80–900 nm, and low thickness films resulted in better photosensors.[1–11] However, the penetration depth of UV light in ZnO thin film (or bulk) is up to 25 nm.[12] Therefore, it would be interesting to explore the photodetection mechanism of a ZnO phototransistor with 25 nm thickness of ZnO thin film as an active channel.

ZnO thin film can be deposited by many potential methods, including spray pyrolysis, electrodeposition, pulsed laser deposition (PLD), metal–organic chemical vapor deposition (MOCVD), thermal evaporation (TE), chemical vapor deposition (CVD), hydrothermal and RF sputtering.[8,12–16] Among these deposition methods, RF sputtering is considered to be more effective because it can produce a uniform deposition of ZnO thin film over a large area, with precise control over the film thickness. It is basically a low-cost technique wherein non-toxic gases are employed during the processing.[16–18] In addition, RF sputtering can be used to decorate several types of substrate surfaces, including silicon, sapphire, glass, ITO coated glass, and flexible polymers, with a thin layer of ZnO.[8,12–18] Among these substrates, IC compatible SiO_2/Si substrate is most important.

Considering the above advantages of phototransistors over conventional photodetectors, and the possibility of improved device performance for low thickness ZnO film grown on IC compatible SiO_2/Si substrate, the fabrication and detailed characterization of a ZnO phototransistor on 25 nm ZnO thin film is carried out in the present study.

EXPERIMENTAL

Materials

All the chemicals employed in the study were purchased from Sigma Aldrich and are used without further purification. During the chemical processes and cleaning of the substrate, deionized water (with the resistivity of 18.2 MΩ cm) was used. An n-type <100> orientation silicon wafer with 0.001–0.005 Ω cm resistivity was used as a substrate material for the device fabrication.

Methods

Deposition of ZnO Thin Film

Before the fabrication of phototransistors, an n-type (100) silicon substrate was cleaned sequentially by using RCA1 and RCA2 processes. On the cleaned substrate, a 200 nm thick silicon dioxide (SiO_2) layer was deposited by dry thermal oxidation in a horizontal tube furnace maintained at 1100°C for 2 h. ZnO thin film on the Si/SiO_2substrates was deposited using RF sputtering in which a high purity ZnO target and the SiO_2/Si substrate were loaded and kept at a distance of 14 cm from each other in the sputtering chamber evacuated to a base pressure of 5×10^{-5} mbar and the processing pressure of 5×10^{-2} mbar was used during the film deposition. For the deposition of single-crystal and high-quality ZnO film, the substrate temperature was gradually increased to 400°C and kept constant throughout the deposition process. With these preliminary settings, the deposition rate, sputtering power, and frequency were also set at 3 nm/min, 100 W, and 13.5 MHz, respectively. The deposition environment was meticulously optimized, to obtain a single-crystal structure of 25 nm ultra-thin ZnO film. After film deposition, the substrate (ZnO/SiO_2/

Si) was diced into pieces. One die of the substrate was used for the fabrication of the phototransistors, and the remaining dies of the substrate were used for the XRD, PL, AFM, and FESEM analysis.

Fabrication of ZnO Phototransistor

After ZnO thin film deposition, a standard semiconductor processing rule was adopted for the fabrication of the bottom-gate phototransistor structure. First, a lift off resist (LOR) + positive photoresist (PPR) was spin-coated on the ZnO/SiO_2/Si substrate. After this, a dark field mask was aligned on the substrate using a SUSS Micro-Tec MJB4 mask aligner, through which the substrate was exposed to light. A pattern was obtained on this substrate by dipping it in an MF319 developer solution for 25 s. On this patterned substrate, metal layers of Cr/Au (20/50 nm) were deposited using thermal evaporation, and the extra metal layer was lifted off with a PG remover. This Cr/Au metal layer works as an alignment mark (reference) for further processing (e.g., drain and source creation) because the ZnO film was very thin and transparent.

Next, a PPR photoresist was spin-coated on the ZnO/SiO_2/Si substrate surface and illuminated through a white field mask and developed in an MF319 solution for 25 s. The developed (patterned) substrate was then dipped in a solution of HCl and DI water (1:30 ratio) to selectively etch out the ZnO; the etching rate was measured to be 2 nm/s. After etching, many isolated rectangular blocks of ZnO were obtained on the substrate. Because of this isolation, a PT fabricated on one island was not electrically connected to another PT, which is fabricated on an adjacent island, causing each transistor to be isolated from one another. Then these islands were treated with hydrogen peroxide by dipping the substrate in a solution composed of one part H_2O_2 and three parts DI water for 5 min. By using similar steps as mentioned during Cr/Au deposition, Ti (20 nm)/Au (80 nm) metal layers for drain and source electrodes were deposited on isolated ZnO islands. The back gates were realized by depositing a Ti/Au layer on the backside of the Si/SiO_2 substrate using e-beam evaporation and photolithography. Proper cleaning of the substrate and the device was performed after each lithography and depositions steps, wherein the substrate was dipped in acetone and IPA solution in a sequence of 5 min each, followed by rinsing with DI water, and drying with N_2 gas.

CHARACTERIZATION METHODS

The ZnO thin film and oxide layer thickness were measured by an ellipsometer (SENTECH Instruments SE 800). An atomic force microscope (AFM) (PICO scan 210; PICO SPM) was used to probe the surface topography of the ZnO thin film. X-ray diffraction (Rigaku SmartLab) was used to investigate the crystal phases in the ZnO thin film. The ZnO thin film surface morphology was studied by using a field-emission scanning electron microscope (FESEM) (ZEISS Ultra 55, Germany). Elements and their co-ordination in the ZnO thin film were investigated by XPS (ULVAC-PHI; PHI5000 Versa Probe II). Photo luminescence (PL) spectroscopy measurement (FluoroMax-4; HORIBA Scientific) was used to find the optical bandgap of the ZnO thin film. The electrical characteristics of the phototransistors under dark and UV illumination were measured using a semiconductor parameter analyser (Keithley 4200-SCS). Phototransistors were illuminated with a commercial low-cost light-emitting diode (365 nm) (L365R-06; Marubeni America Corporation).

RESULTS AND DISCUSSION

Characterization of ZnO Thin Film

Figure 1a shows a two-dimensional AFM image of the RF sputtered ultra-thin (25 nm) ZnO film on SiO_2/n-Si < 100 > substrate. This image exhibits the smoothness, orientation, and uniformity of the film. The AFM images were analyzed using WSxM software, and average surface roughness of ZnO film, RMS roughness, and the average grain size were calculated. The average roughness and the RMS roughness of the film were found to be 0.58 nm and 0.74 nm, respectively, whereas the average grain size of the ZnO thin film was found to be on the order of 17.4 nm. This result indicates that the film surface was smooth, and it has uniformly distributed grains. The surface roughness values of the film are observed to be much smaller than the values of previously reported film,[6] indicating that the film surface was smoother than the reported film.[6] The smooth surface of the film has caused a higher dark and photocurrent compared to reported currents,[9,19] as shown later. The three-dimensional AFM image of the ZnO thin film is shown in Fig. 1b. This image revealed the vertical alignment of the grains. The statistics of the film's grains are given in Fig. 1c.

The field emission scanning electron microscopy (FESEM) image of the ZnO thin film is shown in Fig. 1d. The FESEM image shows that there is uniform distribution of nanoparticles over the substrate and that they are separated from one another with a clear boundary, thus supporting the AFM result. The results also confirm the formation of a good electron-conducting channel between the source and drain of the phototransistor because of limited scattering in the film. An efficient ohmic contact was expected between Ti/Au metal layers and the high-quality film. In view of this, the Ti/Au metal layer was deposited for the source and drain electrode on the film for the fabrication of PT.

Figure 2 illustrates the x-ray diffraction pattern of ZnO thin film measured by high-resolution x-ray diffraction instrument (Rigaku Smartlab 3KW) with Cu-Kα of 1.542 Å wavelength. From the x-ray

Fig. 1. (a) 2D AFM image of the ZnO thin film, (b) 3D AFM image of the ZnO thin film, (c) statistics of the thin film as analysed by AFM, (d) FESEM image of ZnO thin film.

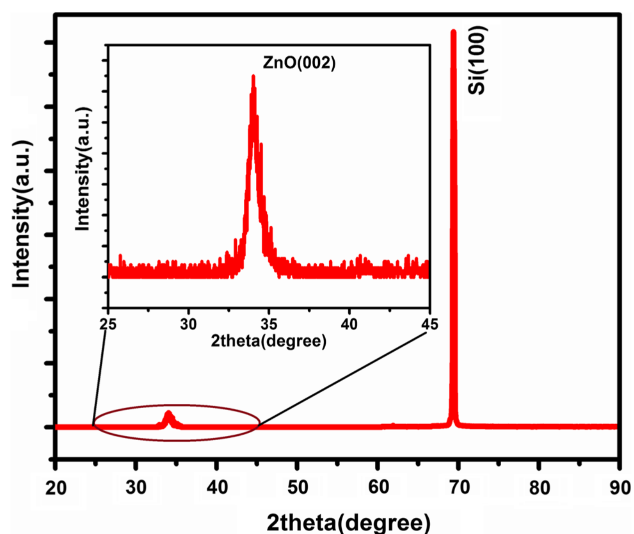

Fig. 2. X-ray diffraction pattern of the ZnO thin film, and the inset represents the ZnO 002 peak.

diffraction pattern, a prominent peak was observed at a 34.5° diffraction angle attributed to the (002) ZnO hexagonal wurtzite crystal phase.[16–19] Another peak was observed at a 69.2° diffraction angle for the (100) plane in the n-Si (100) substrate. Navamathavan et al.[19] have obtained a similar single peak at 34.5° for the ZnO film deposited by RF sputtering. This single peak was obtained by elevating the substrate temperature to 400°C and further the film was used for fabrication of transistor. The intensity of the peak at 34.5° in the present study is larger than the peak intensity of the reported work.[19] Also, the full width half maximum (FWHM) is smaller than the FWHM value of reported film.[19] Thus, the results obtained from the present study states that the crystal structure of the film is much better than that of the previously reported.[19] The crystalline size of the ZnO film was calculated by using Scherer's formula given in Eq. 1:[16–18]

$$D = \frac{c\lambda}{\beta \cos\theta} \tag{1}$$

where D is the crystalline size, C is dimensionless shape factor (~ 0.9), λ is the wavelength of x-ray radiation, β is the full width at half maximum (FWHM), and θ is the diffraction angle. The spacing between the crystal planes was calculated by using[3,20]:

$$\frac{1}{d_{hkl}^2} = \frac{4}{3}\left(\frac{h^2 + hk + k^2}{a^2}\right) + \frac{l^2}{c^2} \tag{2}$$

where a and c are two lattice parameters, and h, k, l, are miller indices.

Assuming first-order diffraction, and by using Eqs. 3 and 4, respectively, lattice parameters a and c, corresponding to (001) and (002) planes, are calculated[20,21]:

$$a = \frac{\lambda}{\sqrt{3}\sin\theta} \tag{3}$$

$$c = \frac{\lambda}{\sin\theta} \tag{4}$$

All the crystal lattice parameters of the ZnO thin film calculated by using Eqs. 1–4 are listed in Table I.

The crystal unit cell c/a ratio of ZnO thin film was calculated to be 1.732. This value was in good agreement with the theoretical value 1.633, and it shows that the film was crystallized in the hexagonal wurtzite structure that belongs to the space group C_{6v}^4/P6_3mc.[3] We observed a slight deviation (0.101) between the theoretical and experimental values of c/a in the present study. This deviation indicates that the film crystal does not possess an ideal hexagonal wurtzite structure.[3] However, this crystal structure was much better than that of previously RF deposited thin-film crystal because the lattice parameters for this film were close to the theoretical values and better than some experimental results.[3,19–24]

Figure 3 presents the PL spectrum of the RF deposited ZnO thin film measured at room temperature by using a 364 nm excitation wavelengths and emission range was set to 250 nm to 600 nm wavelengths. From the PL spectrum, an absorption peak at 365 nm was observed, which was close to the previously reported values, thereby representing the near band edge energy of ZnO.[22] This result reveals that the film can be used for UV light detection applications.

Figure 4a shows the XPS scan survey spectra of our thin film. From XPS survey spectra, three groups of characteristic signals from oxygen (O1s) (521.43–541.30 eV), zinc (Zn2p) (1011.43–1071.31 eV), and carbon (C1s) (276.30–296.30 eV) can be observed. Detailed information about the elemental composition and co-ordination can be derived from the high-resolution section of the survey spectrum in the range of Zn2p (Fig. 4b), O1s (Fig. 4c), C1s (Fig. 4d). From Fig. 4b, two broad highly resolved characteristic signals located at 1021.43 eV and 1044.43 eV were observed form Zn2p3 and Zn2p1, respectively, and for these two morphologies the binding energy difference was found to be 23 eV, thereby representing zinc and oxygen bonding in the ZnO film.[3,24] From Fig. 4c, an O1s high-resolution spectrum that is the interference of three signals in the range 526.02–532.07 eV, was observed, corresponding to oxygen from the surface and within the film. The oxygen in the bulk of the ZnO film is generally responsible for PPC in conventional metal-oxide semiconductor-based photodetectors.[8] The intensity count of the O1s characteristic signal at 530.0 eV was larger compared to intensity counts at 531.0 eV and 532.0 eV, respectively.[25] The oxygen vacancy of the thin film can thus be calculated as the ratio of the intensity of characteristics signal at 531.0 eV and 530.0 eV. The calculated value of V_0 was found to be 0.37 and it is in agreement with the reported results.[25] The peak

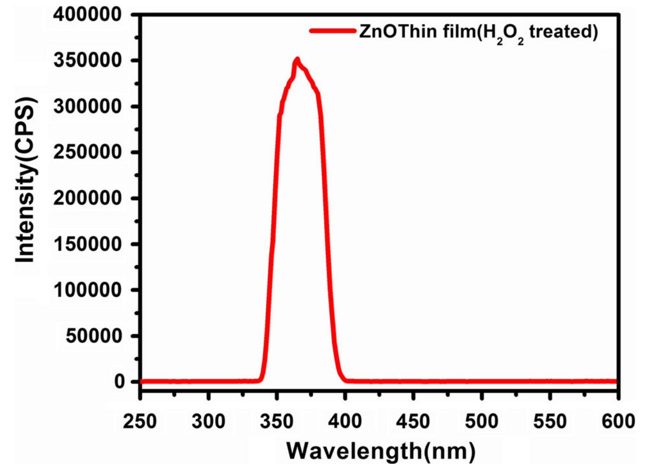

Fig. 3. PL spectrum of the ZnO thin film.

Table I. Lattice parameters calculated by using XRD data

Layer thickness	2θ	Lattice parameter a (nm)	Lattice parameter c (nm)	FWHM (°)	Crystalline size (nm)
25 nm	34.5	0.3002	0.5200	0.9386	11.42

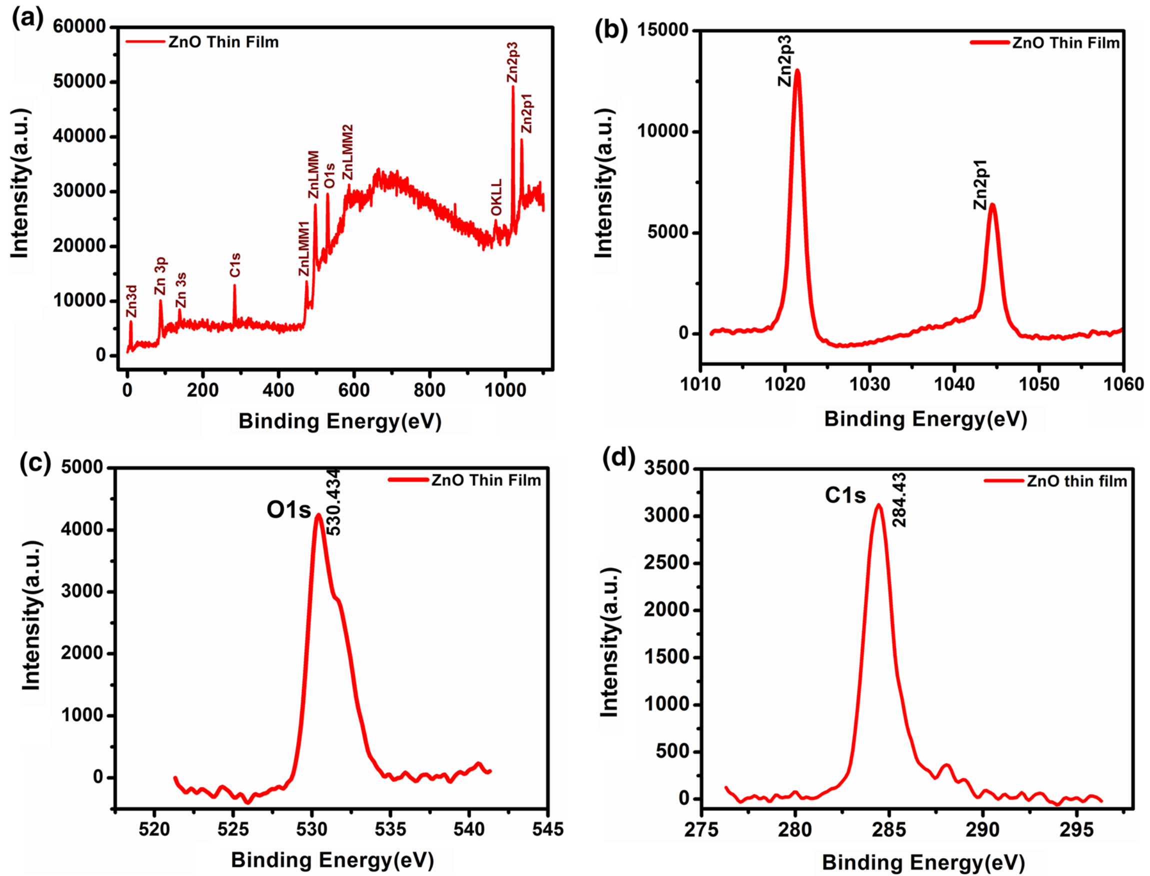

Fig. 4. XPS spectrum of the ZnO film, (a) survey spectra of the ZnO thin film, (b) Zn-2p spectrum of the ZnO thin film, (c) O1s spectrum of the ZnO thin film, (d) carbon spectrum of the ZnO thin film.

located at 530.43 eV shown in Fig. 4c can be attributed to Zn-OH bonding.[18] This surface oxygen of the film is probably responsible for large photocurrent under UV light illumination. Therefore, it is predicted that the photocurrent in phototransistor or conventional two-terminal photodetector can increase with increasing surface oxygen or by decreasing the oxygen deficiency in the bulk. The characteristics signal of spectrum at 530.43 eV was associated with bulk oxygen, representing that the O^{2-}ion is surrounded by Zn^{2+} ion or vice versa.[3,25] From Fig. 4d, the C1s spectrum is a superposition of three feature characteristic signals, 285.4 eV, 286.7 eV, and 289.1 eV, respectively. The first signal corresponds to carbon atoms in the hydrocarbon, second characteristics signal associated with carbon atoms in C–O bond, and the last characteristic signal was associated with carbon atoms in C=O bonds.[3,25] The C1s peak of the ZnO thin film from Fig. 4d is observed to be at 284.43 eV.[18]

Electrical and Optical Properties of ZnO Transistors

A schematic diagram of the phototransistors is shown in Fig. 5a, and their real microscopic images, which were measured by using a high-resolution optical microscope (Olympus MX61-F), is shown in Fig. 5b–c. The measured values of the W/L ratio of the two phototransistors are 263 μm/100 μm and 461 μm/100 μm, respectively.

The transfer and output characteristics of the phototransistors in the dark as well in UV light irradiation are shown in Fig. 6a–d. Semi-logarithmic transfer characteristics of the two PTs are shown in the inset of Fig. 6c–d. Our phototransistors are a typical metal-oxide channel and were operating in the enhancement-mode, as can be observed from Fig. 6a–d. These basic PT characteristics can be used to calculate the low-field mobility and transconductance. The transconductance of the two phototransistors are calculated to be $1.5 \times 10^{-7} S$ (W/L = 263/100), and $3.5 \times 10^{-7} S$ (W/L = 461/100), respectively. The channel electron mobility of the fabricated phototransistors can be calculated using the formula[26]:

$$\mu_l = \frac{Lt}{W\varepsilon_0\varepsilon_r}\frac{dI_{ds}}{dV_g} \quad (5)$$

where μ_l is the low-field electron mobility, t is the thickness of the channel, V_g is the gate voltage, I_{ds} is the channel current, ε_0 and ε_r are the permittivity of the free space and relative permittivity of ZnO, W is

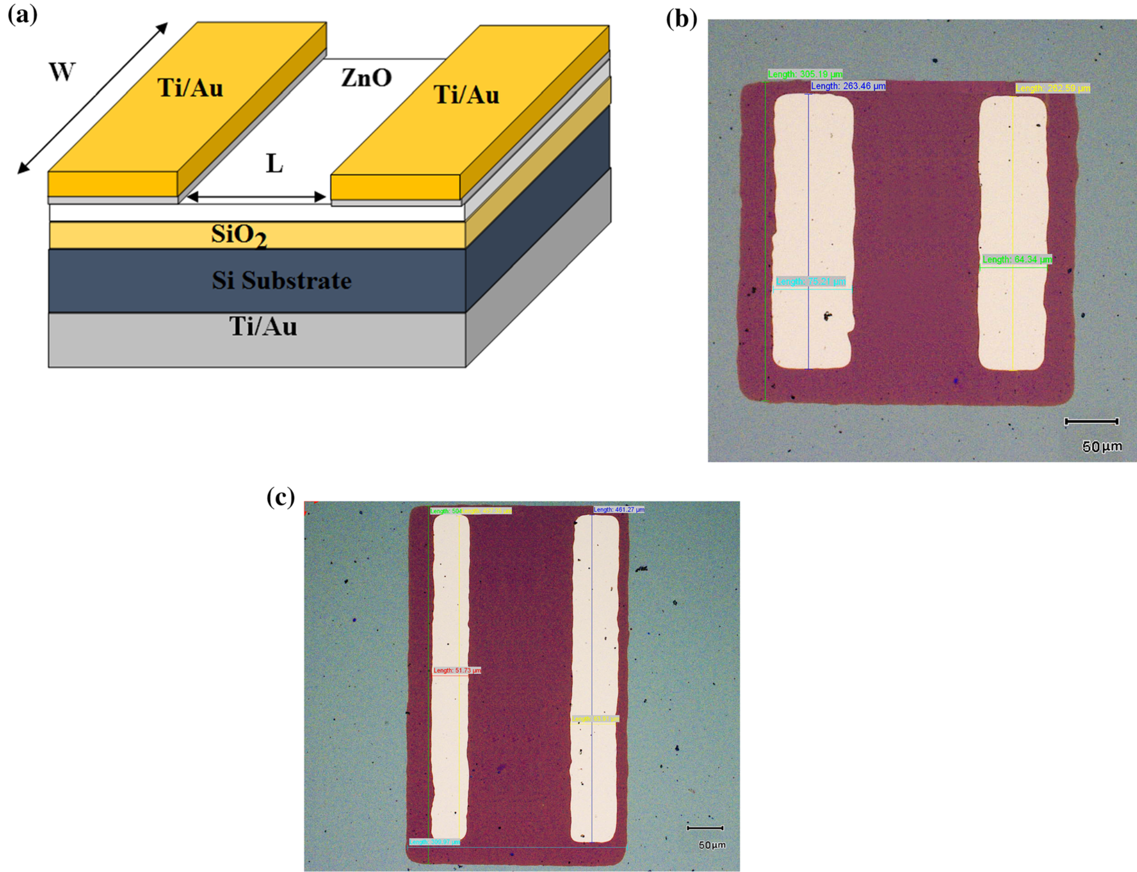

Fig. 5. (a) Schematic representation of the phototransistor, (b) microscope image of the fabricated phototransistor with W/L ratio 263 μm/100 μm, (c) microscope image of the fabricated phototransistor with W/L ratio 461 μm/100 μm.

the width of the phototransistor. The differential term in Eq. 5 is the transconductance of the fabricated phototransistor. The low-field mobilities of the phototransistors are calculated to be 4.92 cm^2/V s (W/L = 263/100) and 4.52 cm^2/V s (W/L = 461/100), respectively. From Fig. 6a–d, PT with W/L $\sim$ 461/100 shows a larger photo and dark current than PT with $W/L \sim$ 263/100, and this result is in agreement with reported results.[23]

From Fig. 6a and b at higher drain voltages, the drain current is parallel to the voltage axis exhibiting hard saturation for both the phototransistors.[23] At hard saturation points the channel can be fully depleted by applying suitable biasing voltage.[23] These phototransistors can be efficiently applied in several circuits because of their high output impedance.

The on–off current ratios of two phototransistors were obtained from the inset of Fig. 6c and d. The values of the on–off currents ratio for these two transistors are 2.6 $\times$ 10^6 (461/100), 2.1 $\times$ 10^4 (263/100), respectively. From Fig. 6a–d, it can be seen that both the phototransistors are sensitive to UV light. The contrast ratio of these two phototransistors is 2 ($W/L \sim$ 263/100) and 1.5 (W/L = 461/100), respectively. These low contrast values were because of the low-power LED ($\sim$ 1 mW/cm^2) light source used to probe the photodetection capability of these two transistors. The responsivities of the phototransistors are calculated by[26]:

$$R = \frac{I_p - I_d}{PS} \tag{6}$$

where I_p and I_d are the photo and dark current of the phototransistor, P is photon intensity, S is the effective area of the phototransistor. The zero gate bias voltage responsivities of these two phototransistors are calculated to be 1.187 A/W (of PT with $W/L \sim$ 263/100) and 0.999 A/W (of PT with $W/L \sim$ 461/100), respectively. These values were larger than the previously reported values.[9,22–27] The detectivity of the two transistors representing the sensitivity of the photodetector to UV light, is calculated by[26]:

$$D = \frac{S^{1/2}}{e^{1/2} I_d^{1/2}} R \tag{7}$$

where D is the detectivity, is the effective area, R is the responsivity, e is an elementary charge, and I_d is the dark current. The values of detectivity (Jones) of these transistors are calculated to be 3.85 $\times$ 10^{10}($W/L \sim$ 263/100), and 3.35 $\times$ 10^{10} ($W/L \sim$ 461/100),

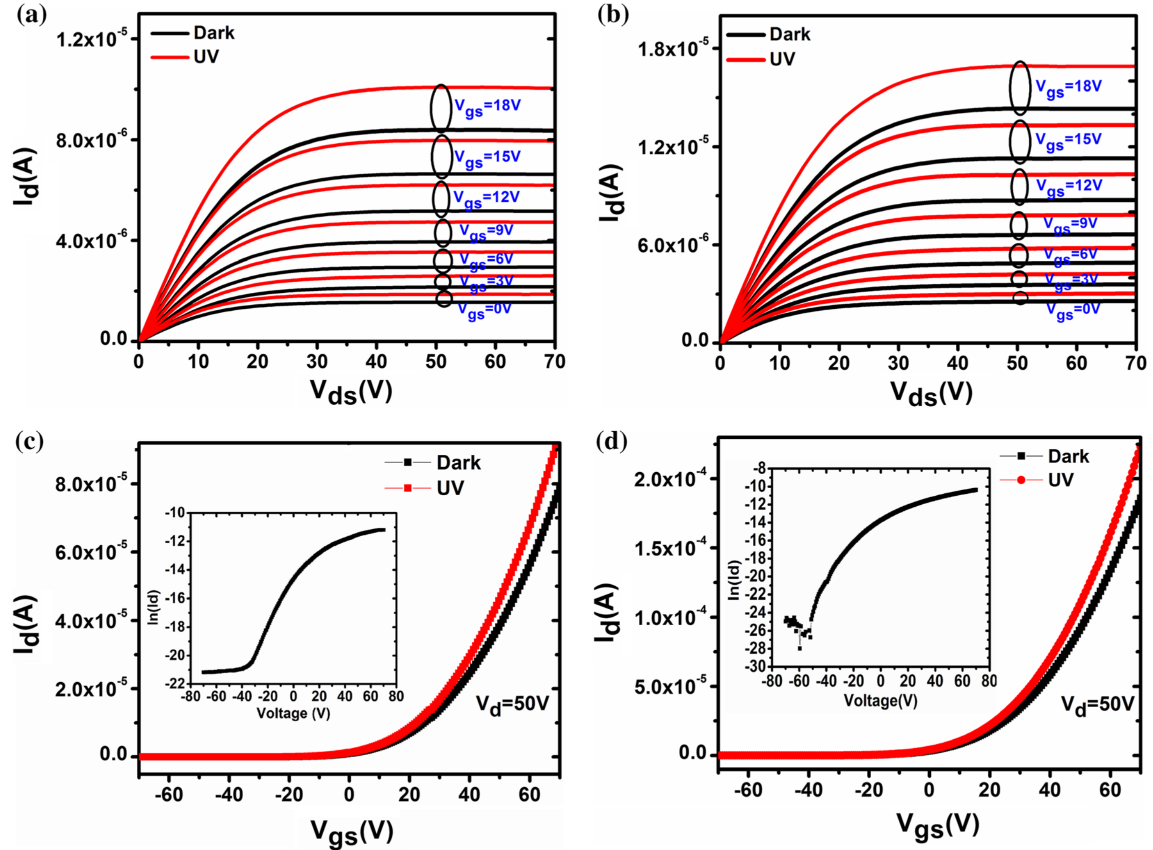

Fig. 6. (a) Output characteristics of the transistor with (W/L) 263/100, (b) output characteristics of the transistor with (W/L) 461/100, (c) transfer characteristics of the transistor with (W/L) 263/100, inset showing the semi-logarithmic plot of transfer characteristics, (d) transfer characteristics of the transistor with (W/L) 461/100, inset showing the semi-logarithmic plot of transfer characteristics.

Table II. Effect of active channel thickness on photodetector performance

Sample No.	Responsivity (A/W)	Detectivity (Jones)	ZnO thickness (nm)	Source of light	References
1.	0.001	–	250	60mW/cm2	11
2.	0.04	–	166	Lamp	28
3.	0.0005	–	100	20mW/cm^2	29
4.	1.34	–	80	Lamp	30
5.	1.99	3.35×10^{10}	25	LED	Present work

respectively. These values are higher than some reported values to date.[26]

The photo-sensing mechanism of the ZnO film is not revealed completely, though it is believed that the change in conductivity of the ZnO film under light illumination, which is responsible for large photocurrent in the ZnO-based photodetector, is caused by the desorption of surface oxygen and exciton generation.[10] Note that oxygen is adsorbed on the ZnO surface by trapping two electrons. When ZnO is illuminated, holes get separated from the excitons and move to the surface and desorb the adsorbed oxygen, resulting in the release of trapped electrons. Finally, these released electrons increase the conductivity of the ZnO thin film, and hence, large photocurrent is generated in the channel for same biasing conditions.[10,20]

The developed phototransistors in the present study are able to detect low-power UV light efficiently. Therefore, they can be used in long-distance optical communication as well as in the integration of photonics and electronics in present CMOS technology. These PTs on a chip can be used as a detector as the thickness of their channel is very thin, which requires less material and areal space, thus they can detect low power light. In addition, thinner film-based photodetectors performed better compared to thicker film-based photodetectors. This

can be stated by the comparison of the results of some previous work summarized in Table II.

CONCLUSION

In this work, phototransistors with ultra-thin ZnO film (with thickness equal to the penetration depth of UV light) as an active channel were fabricated and characterized. The ZnO thin film was deposited by using RF sputtering method on IC compatible SiO_2/n-Si substrate. The performance of phototransistors was found to be dependent on surface morphology, crystal phases, elemental composition, resistivity, mobility, and carrier concentration of ZnO thin film. The characteristic properties of the thin film were investigated by AFM, XRD, PL, and XPS. The resulting phototransistors demonstrated an enhanced photo performance compared to thick channel-based devices reported previously in the literature. Thus, it is concluded that a phototransistor comprising an ultra-thin film as an active channel can find potential applications in the integration of electronics and photonics for long-distance optical communication.

ACKNOWLEDGMENTS

The authors would like to acknowledge the Indian Nanoelectronics User Program (INUP) of the Indian Institute of Technology Bombay (IITB), Bombay, for providing all the necessary analytical equipment facilities to carry out the experimental work.

REFERENCES

1. S.K. Shaikh, S.I. Inamdar, V.V. Ganbavle, and K.Y. Rajpure, *J. Alloys Compd.* 664, 242 (2016).
2. Y.Z. Chiou and J.J. Tang, *Jpn. J. Appl. Phys.* 43, 4146 (2004).
3. U. Ozgür, Y.A. Alivov, C. Liu, A. Teke, M.A. Reshchikov, S. Dogan, V. Avrutin, S.J. Cho, and H.A. Morkoc, *J. Appl. Phys.* 98, 041301 (2005).
4. S.J. Pearton, D.P. Norton, K. Ip, Y.W. Heo, and T. Steiner, *J. Vac. Sci. Technol. B* 22, 932 (2004).
5. A.B. Yadav, A. Pandey, and S. Jit, *Acta Metall. Sin. (English. Lett.)* 27, 682 (2014).
6. B. Hanna, K.P. Surendran, and K.N. Narayanan Unni, *RSC Adv.* 8, 37365 (2018).
7. A. Rajan, H.K. Yadav, V. Gupta, and M. Toma, *J. Mater. Sci.* 48, 7994 (2013).
8. S. Lee, S.-E. Ahn, Y. Jeon, J. Ahn, I. Song, S. Jeon, D. Jin Yun, J. Kim, H. Choi, U. Chung, and J. Park, *Appl. Phys. Lett.* 103, 251111 (2013).
9. H.-Y. Liu and R.-C. Huang, *IEEE Electron. Dev. Lett.* 40, 243 (2019).
10. K. Lee, K. Kim, J.M. Choi, M.S. Oh, D.K. Hwang, S. Jang, E. Kim, and S. Im, *J. Phys. D Appl. Phys.* 41, 135102 (2008).
11. H.K. Yadav, K. Sreenivas, and V. Gupta, *J. Appl. Phys.* 107, 044507 (2010).
12. B.S. Sannakashappanavar, A.B. Yadav, C.R. Byrareddy, and N.V.L.N. Murty, *Mater. Res. Express* 6, 116445 (2019).
13. R. Ahmad, N. Tripathy, N.K. Jang, G. Khang, and Y.B. Hahn, *Sens. Actuators B* 206, 146 (2015).
14. N. Liu, G. Fang, W. Zeng, H. Zhou, F. Cheng, Q. Zheng, L. Yuan, X. Zou, X. Zhao, and A.C.S. Appl, *Mater. Interfaces* 7, 1973 (2010).
15. A. Anta, E. Guillén, and R. Tena-Zaera, *J. Phys. Chem. C* 116, 11413 (2012).
16. A.B. Yadav and B.S. Sannakashappanavar, *J. Alloys Compd.* 770, 701 (2019).
17. A.B. Yadav, P.V.L. Parvathi, and R.T. Shaik, *Thin Solid Films* 685, 343 (2019).
18. B.S. Sannakashappanavar, C.R. Byrareddy, N.A. Pattanashetti, K. Singh, and A.B. Yadav, *J. Nanoelectron. Optoelectron.* 14, 964 (2019).
19. R. Navamathavan, J.H. Lim, D.K. Hwang, B.H. Kim, J.Y. Oh, J.H. Yang, H.S. Kim, and S.J. Park, *J. Korean Phys. Soc.* 42, 271 (2006).
20. R. Menon, K. Sreenivas, and V. Gupta, *J. Appl. Phys.* 103, 094903 (2008).
21. M.I. Medina-Montes, H. Arizpe-Chávez, L.A. Baldenegro-Pérez, M.A. Quevedo-López, and R. Ramírez-Bon, *J. Electron. Mater.* 41, 1962 (2012).
22. A. Srivastava and N. Kumar, *J. Electron. Mater.* 46, 4842 (2017).
23. E. Flores-García, P. González-García, and R. Ramírez-Bon, *J. Electron. Mater.* 47, 5537 (2018).
24. K.J. Hong, T.S. Jeong, and T.S. Kim, *J. Electron. Mater.* 46, 425 (2017).
25. R.L. Hoffman, B.J. Norris, and J.F. Wager, *Appl. Phys. Lett.* 82, 733 (2003).
26. H. Choi, S. Seo, J.H. Lee, S.H. Hong, J. Song, S. Kim, S.Y. Yim, K. Lee, S.J. Park, and S. Lee, *J. Mater. Chem. C.* 6, 6014 (2018).
27. J.Y. Li, S.P. Chang, M.H. Hsu, and S.J. Chang, *Materials* 10, 126 (2017).
28. F. Yakuphanoglu and S. Mansouri, *Microelectron. Reliab.* 51, 2200 (2011).
29. S. Park, B.J. Kim, and S.J. Kang, *J. Korean Phys. Soc.* 73, 1351 (2018).
30. N. Zebbar, L. Chabane, N. Gabouze, M. Kechouane, M. Trari, M.S. Aida, S. Belhousse, and F. HadjLarbi, *Thin Solid Films* 605, 89 (2016).

Publisher's Note Springer Nature remains neutral with regard to jurisdictional claims in published maps and institutional affiliations.